Progress in Neurobiology 184 (2020) 101699

Contents lists available at ScienceDirect

Progress in Neurobiology

journal homepage: www.elsevier.com/locate/pneurobio

Original Research Article

Connectional gradients underlie functional transitions in monkey pre-supplementary motor area

Davide Albertini[a,*,1], Marzio Gerbella[a,*,1], Marco Lanzilotto[a,c], Alessandro Livi[a,b], Monica Maranesi[a], Carolina Giulia Ferroni[a], Luca Bonini[a,*]

[a] Department of Medicine and Surgery, University of Parma, via Volturno 39, 43125, Parma, Italy
[b] Department of Neuroscience, Washington University in St. Louis, MO, 63110, USA
[c] Department of Psychology, University of Turin, via Verdi 10, 10124, Torino, Italy

ARTICLE INFO

Keywords:
Neuroanatomy
motor control
Action observation
Mirror neuron
Pre-sma

ABSTRACT

The pre-supplementary motor area F6 is involved in a variety of functions in multiple domains, from planning/withholding goal-directed actions in space to rule-based cognitive processes and social interactions. Yet, the neural machinery underlying this functional heterogeneity remains unclear. Here, we measured local population dynamics in different rostro-caudal sites of cytoarchitectonically verified area F6 in two monkeys during spatial, contextual and motor processes, both in individual and social conditions. Then, we correlated multimodal population tuning with local anatomical connectivity revealed by neural tracer injections into the functionally characterized sites. We found stronger tuning for object position relative to the monkey in the rostral portion of area F6 than in its caudal part, which in turn exhibits stronger tuning to self and other's (observed) action. Functional specificities were associated with a rostro-caudal transition in connectivity strength from lateral prefrontal cortex, pregenual anterior cingulate cortex and associative striatum (rostrally), to dorso-ventral premotor areas and the motor putamen (caudally). These findings suggest that the functional heterogeneity of the pre-supplementary area F6 is accounted for by gradual transitions in functional properties grounded on local cortico-cortical and cortico-striatal connectional specificities.

1. Introduction

The pre-supplementary motor area (called F6 in the monkey, see Matelli et al., 1991; Luppino et al., 1991) lies in the mesial wall of the cerebral hemispheres, rostrally to the supplementary motor area (Matsuzaka et al., 1992; Picard and Strick, 1996). It receives inputs from prefrontal and cingulate cortex and sends projections to parieto-dependent areas of the dorsal and ventral premotor cortex (Rizzolatti and Luppino, 2001; Johansen-Berg et al., 2004; Morecraft et al., 2012), hence being optimally placed for "linking cognition to action" (Nachev et al., 2008), and to act as a hub for processes related with motor intentionality (Zapparoli et al., 2018). Its involvement in a so wide set of functions, ranging from planning of goal-directed actions in space to rule-based cognitive processes and social interactions, makes it "the most frequently activated region" in human brain imaging studies (Behrens et al., 2013).

Indeed, pioneering neurophysiological studies with ethological techniques in the monkey suggested that area F6 plays a role in the preparation of reaching–grasping arm movements and in their release when appropriate conditions are set (Rizzolatti et al., 1990). Subsequent studies showed that this area is also involved in higher-order control processes (Picard and Strick, 2001; Isoda and Hikosaka, 2007), including updating of motor plans (Shima et al., 1996), selecting effector-independent actions (Fujii et al., 2002), organizing and learning complex motor sequences (Tanji and Shima, 1994; Tanji, 2001), and planning or controlling reaching-grasping actions (Lanzilotto et al., 2016). Recent studies also indicate that F6 plays a role in social behavior and is part of a brain network dedicated to the processing of social interactions (Sliwa and Freiwald, 2017). In this regard, single neuron evidence indicates that F6 neurons can exhibit remarkable selectivity for self- and/or others' actions (Yoshida et al., 2011; Livi et al., 2019), others' future choices (Falcone et al., 2017), and even for observed objects depending on whether they constitute potential targets for self and/or others' action (Livi et al., 2019). In the light of these findings, it should not be surprising that the neural mechanisms underlying the functional heterogeneity of the pre-supplementary motor cortex remain

* Corresponding authors.
E-mail addresses: davide.albertini@unipr.it (D. Albertini), marzio.gerbella@unipr.it (M. Gerbella), luca.bonini@unipr.it (L. Bonini).
[1] These authors equally contributed to the work.

https://doi.org/10.1016/j.pneurobio.2019.101699
Received 11 April 2019; Received in revised form 6 September 2019; Accepted 18 September 2019
Available online 23 September 2019

largely unclear. Nonetheless, two main hypotheses have been proposed concerning its anatomo-functional organization: 1) F6 is a unitary, essentially homogeneous, anatomo-functional area (e.g. (Rizzolatti and Luppino, 2001)), which underlies a specific but still unclear functional signature, or 2) it indexes a variety of functional properties linked with gradual rostro-caudal transitions in local connectional specificities (Nachev et al., 2008).

In the present study, we addressed these questions by combining neurophysiological and neuroanatomical techniques in macaque monkeys. First, we characterized local population dynamics in different rostro-caudal sites of area F6 in two monkeys using a large set of tasks and conditions recently employed in separate single neuron experiments (Lanzilotto et al., 2016; Livi et al., 2019). We found stronger tuning of rostral area F6 to the distance of target objects from the monkey relative to the caudal one, which in turn exhibits stronger tuning to one's own executed action and to observed actions performed by others. Then, we injected neural tracers into each functionally characterized site, revealing a rostro-caudal transition in connectivity strength with lateral prefrontal, pregenual anterior cingulate cortex and striatum/anterior putamen preferentially linked with rostral area F6, whereas dorso-ventral premotor areas and the caudal putamen mostly connected with its caudal part. Our findings favor the idea that area F6 indexes a multiplicity of functions by gradual transitions in local connectional specificities rather than subserving a unique and homogeneous functional signature.

2. Materials and methods

Experiments were carried out on two purpose-bred, socially housed male macaque monkeys (Mk1, Macaca nemestrina, 9 kg, and Mk2, Macaca mulatta, 7 kg). Before recordings, monkeys were habituated to sit in a primate chair and to interact with the experimenters. Then, they were trained to perform the visuomotor tasks described below using the hand contralateral to the hemisphere to be recorded. When the training was completed, a head fixation system was implanted under general anesthesia (ketamine hydrochloride, 5 mg/kg, i.m., and medetomidine hydrochloride, 0.1 mg/kg, i.m.), followed by postsurgical pain medications (see (Bruni et al., 2015) for details). Two arrays of linear silicon probes were implanted in area F6 of each monkey at two different antero-posterior positions of the left (Mk1) or right (Mk2) hemisphere. At the end of the recordings, the probes were removed and antero-retrograde neural tracers were injected, in correspondence with the position previously occupied by each of the explanted probes. All experimental protocols complied with the European law on the humane care and use of laboratory animals (directives 86/609/EEC, 2003/65/CE, and 2010/63/EU), were authorized by the Italian Ministry of Health (D.M. 294/2012-C, 11/12/2012 and 48/2016-PR, 20/01/2016), and were approved by the Veterinarian Animal Care and Use Committee of the University of Parma (Prot. 78/12, 17/07/2012 and Prot. 91/OPBA/2015).

2.1. Apparatus and behavioral paradigm

Both monkeys were trained to perform an Execution task (Fig. 1A, EXE) as well as to observe the same task performed by an experimenter in their peripersonal (Fig. 1A, OBSp) and extrapersonal (Fig. 1A, OBSe) space. These tasks have been described in details in previous works (see (Lanzilotto et al., 2016; Livi et al., 2019)).

Briefly, during EXE, the monkey was seated on a primate chair in front of a box, divided horizontally into 2 sectors by a half-mirror where a spot of light (fixation point) was projected in the exact position of the center of mass of the not-yet-visible target object. The objects (a ring, a small cone, and a big cone) afforded three different grip types (hook grip, side grip, whole-hand prehension). They were presented randomly, one at a time, at a reaching distance from monkey's hand starting position. The task included two basic conditions (Go and No-Go), and each trial was preceded by a variable (from 1 to 1.5 s) inter-trial period.

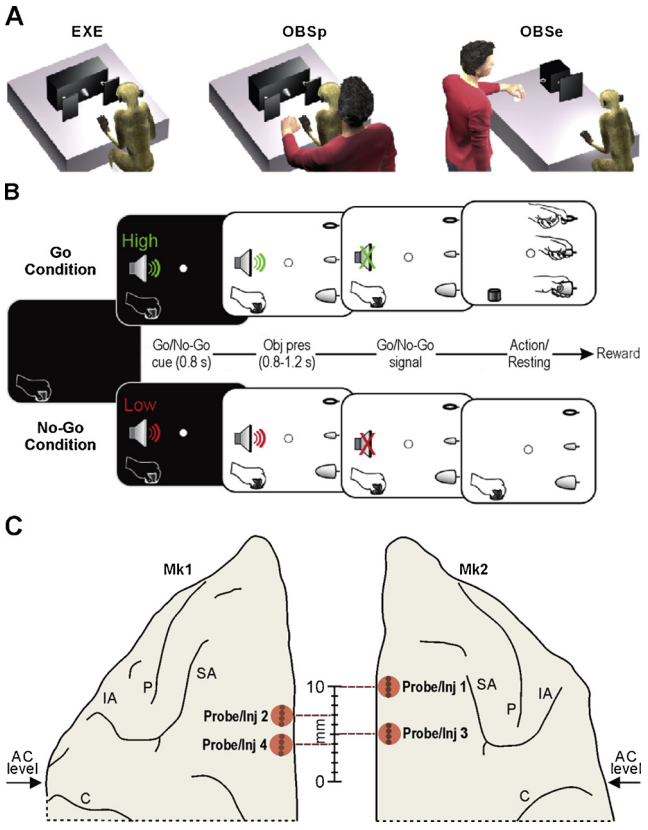

Fig. 1. Behavioral tasks and investigated regions. (A) Schematic representation of the three tasks: execution (EXE), observation in the monkey's peripersonal (OBSp) and extrapersonal (OBSe) space. **(B)** Temporal sequence of task events. **(C)** Recorded and injected sites. The gray dots illustrate the anatomical location of each probe's shafts and the red shaded circles indicate the location of the core of injection sites relative to the implanted probes. Anatomical position of the injections is defined relative to their distance from the anterior commissure (AC). The scale of Mk2 applies also to Mk1. Abbreviations: C, central sulcus; IA, inferior arcuate sulcus; P, principal sulcus; SA, superior arcuate sulcus.

1 *Go condition* (Fig. 1B). The fixation point was presented and the monkey was required to start fixating it within 1.2 s. Fixation onset resulted in the presentation of a cue sound (high tone, 1200 Hz), which instructed the monkey to grasp the subsequently presented object (Go cue). After 0.8 s one of the objects became visible. Then, after a variable time lag (0.8–1.2 s), the sound ceased (Go signal), and the monkey had to reach, grasp, and pull (for 0.8 s) the object within 1.2 s to get a fixed amount of juice reward (automatically delivered). During another set of trials (grasping in the dark) the light was switched off automatically with the Go signal and the monkey performed the action in complete darkness.
2 *No-Go condition* (Fig. 1B). The sequence of task events in this condition was the same as in the Go condition but a different cue sound (low tone, 300 Hz) instructed the monkey to remain still and fixate the object for 1.2 s in order to receive the reward.

The same sequence of events described for EXE also applied to OBSp and OBSe. The task phases were automatically controlled and monitored by LabView-based software, enabling the interruption of the trial if the monkey broke fixation, made an incorrect movement, or did not respect the task temporal constraints. In all these cases, no reward was delivered. Failed trials were repeated until at 10 trials were collected

for each condition.

2.2. Recording techniques

Neuronal recordings were obtained from 4 multi-shaft 3D arrays of linear silicon probes with 8 recording sites per shaft and 2 parallel modules of 4 shafts per probe (64 channels per probe). The recording sites were spaced by 500 µm, along the 8 mm shank with a rectangular section of 80 µm (width) x100 µm (thick). Each shaft was spaced by 550 µm from the adjacent one, and each 4-shaft module was spaced apart from the other by 350 µm (see Fig. 7 in (Barz et al., 2017)). These probes were implanted for previous studies (Lanzilotto et al., 2016; Livi et al., 2019), and details on the methodology of probe fabrication, assembly and implantation have been described elsewhere (Barz et al., 2017; Bonini et al., 2014; Ferroni et al., 2017). The signal was amplified and sampled at 40 kHz with a 16-channel Omniplex recording system (Plexon). Different sets of 16 channels were recorded only one time during separate sessions in different days. All signal analyses were performed off-line with fully automated software (MountainSort, Chung et al. 2017, available online at https://github.com/magland/mountainlab), considering both single- and multi-unit activity (referred to as "units", see (Lanzilotto et al., 2019) for details on spike sorting procedures). Furthermore, to exclude that possible artifacts were counted as spikes, we automatically inspected all waveforms of all isolated units and retained, for each one, only those waveforms that did not exceed ± 3 SD from the average waveform in all data points (for each unit, about 10% of the spikes were removed in this procedure).

2.3. Recording of behavioral events and definition of the epochs of interest

Contact sensitive devices (Crist Instruments) were used to detect when the monkey (grounded) touched the metal surface of the starting position or one of the target objects. To signal the onset and tonic phase of object pulling, an additional device was connected to the switch located behind each object. Custom-made LabView-based software was used to monitor the monkey's performance and to control the presentation of auditory and visual cues (see for details (Bonini et al., 2014)). Eye position was monitored in parallel with neuronal activity with an eye tracking system (Livi et al., 2019): the monkey was required to maintain its gaze on the fixation point (tolerance radius 5°) throughout the task. Off-line analysis of electromyographic activity of proximal and distal forelimb muscles during EXE, OBSp and OBSe has been previously described in both monkeys (Livi et al., 2019), and allowed us to exclude the possible presence of preparatory motor activity during No-Go trials, observation trials and baseline epochs.

Based on the available events and leveraging the same structure shared by all tasks, we focused the analyses on 4 main epochs, identical across tasks: 1) baseline (500 ms before cue sound onset), 2) cue sound (from 100 to 600 ms after sound onset), 3) object presentation (from 100 to 600 ms after light onset) and 4) Go/No-Go signal (from the end of the cue sound to 1000 ms after this event).

2.4. Analyses of the neuronal activity

2.4.1. Sliding window ANOVA

The spiking activity of each unit in all the available trials was compared across conditions (Go/No-Go, objects, Light/Dark) with one-way repeated measures ANOVAs ($p < 0.05$, uncorrected) in 200 ms bins, advanced in steps of 20 ms for the entire period of interest relative to 1) object presentation (from -1300 to 700 ms) and 2) Go/No-Go signal (from -300 to 1200 ms). In the analyses of Go/No-Go and light/dark conditions the trials with the different objects were collapsed, whereas in the analyses of object tuning ANOVAs were carried out within Go and No-Go conditions, separately. The bin-by-bin percentage of significantly tuned units was smoothed with a 60 ms Gaussian kernel to improve visualization. To identify when and for how long the percentage of tuned units was different between subpopulations (rostro-caudal or dorso-ventral) in each monkey, we used bin-by-bin sliding chi-square tests ($p < 0.05$, uncorrected).

2.4.2. Principal component analysis (PCA)

Trial-averaged firing rates of each unit were calculated from -1800 to +1600 ms relative to Go/No-Go signal for all conditions and tasks. The spiking activity was first binned in 20 ms time windows and the resulting firing rates were subsequently smoothed with a 200 ms Gaussian kernel. Then, for each unit, the smoothed firing rates were first divided by the maximum firing rate across all conditions and tasks, and then the overall average firing rate was subtracted bin-by-bin to obtain the normalized firing rate. After this pre-processing, we considered the normalized firing rates as an N-dimensional neural population state space. Since the amplitude of a generic population vector with respect to any arbitrary baseline grows as $\sqrt{N}$ (the mean line segment length in an N-dimensional cube grows as $\sqrt{N}$, see (Anderssen et al., 1976)), we normalized each firing rate dividing it for $\sqrt{N}$ to compare reliably PCA projections of different subpopulations even if they were made up of a different number of units. Then, PCA was performed including all conditions (i.e. Go/No-Go, object, light/dark) and tasks (EXE, OBSp, OBSe). For each condition and in each task, we then projected the corresponding full-dimensional neural trajectory onto the plane of the first two PCs (the projections of different objects were remarkably similar and were thus averaged) obtaining a two-dimensional curve that describes the evolution of the population state along the trial for that particular task and condition. To mark the time corresponding to specific task events (i.e. start of trial, object presentation, Go/No-Go signal, pulling, reward) along the trajectories, we calculated their mean time relative to the Go/No-Go signal of each condition.

2.4.3. Hierarchical cluster analysis

To evidence the possible relationship among neural representation of tasks and conditions we performed a hierarchical cluster analysis. Given a certain neural population of N units, firing rates of all units were calculated binning the spiking activity and averaging it across trials. We created a firing rate matrix F with N rows and $c{\cdot}t$ columns (where c is the number of conditions and t the number of time points per condition within the epoch of interest). Then, we computed the Mahalanobis linkage distances (Matlab function: manova1) between the activities in the N-dimensional state space of all possible pairs of conditions in the epoch of interest. Since the Mahalanobis distance between any pair of arbitrarily selected conditions increases linearly as a function of the number of units in the population (see Fig. S1), the resulting matrix of distances was normalized dividing it by N. Finally, normalized distance matrix was used to create a hierarchical cluster tree based on the average linkage criterion (Matlab function: manovacluster), presenting the cluster solutions in the form of dendrograms. While building the dendrograms, we sorted the leafs within a branch on the basis of their average distance to nearest branches (Matlab function: optimalleaforder).

2.4.4. Measures of local relevance of functional properties

To isolate and quantify the rostro-caudal functional changes within F6, we computed the Mahalanobis distance in the neural state space of each probe between all levels of specific factors in selected epochs. Specifically, we considered the factors 1) task context, 2) Go/No-Go and 3) Object/grip. Out of the 27 resulting combinations (see Fig. S6), seven of them allowed us to isolate specific "functional dimensions", as follows.

1) Object position. Mahalanobis distance between EXE and OBSe (regardless of the type of object and Go/No-Go condition), during object presentation epoch. Note that a similar measure could be

obtained by contrasting OBSp (where, however, another agent is present close to the monkey) and OBSe, which indeed produce similar results (Fig. S6).
2) Experimenter position. Mahalanobis distance between OBSp and OBSe during baseline, when the monkey is aware of the presence of another agent located either far from or near it but no other confound is present.
3) Agent. Mahalanobis distance between EXE and OBSp (involving the same space sector) during baseline (no additional confound), when the monkey knows who will act because the tasks are run in blocks.
4) Object/Grip. Mahalanobis distance between all possible pairs of objects (averaged) in the Go condition of EXE during the period ranging from object presentation to the end of the Go/No-Go signal epoch.
5) Go/No-Go condition in OBSe. Mahalanobis distance between Go and No-Go conditions in OBSe during Go/No-Go signal epoch, when the observed action occurs.
6) Go/No-Go condition in OBSp. Mahalanobis distance between Go and No-Go conditions in OBSp during Go/No-Go signal epoch, when the observed action occurs.
7) Go/No-Go condition in EXE. Mahalanobis distance between Go and No-Go conditions in EXE during Go/No-Go signal epoch, when the action is performed.

To test statistically the significance of observed rostro-caudal differences in the selected functional dimensions we applied a subsampling procedure. For each dimension, we randomly subsampled without replacement the N units recorded from each probe by selecting $M = N^{2/3}$ units and re-calculating the Mahalanobis distance on this data set: we run this procedure 1000 times and calculated the standard deviation (multiplied by $\sqrt{M/N}$ in order to consider the different size of the subsample with respect to the whole population) of the resulting distribution, taken as standard error. Finally, to test whether the Mahalanobis distances associated to a given functional dimension differed across probes, we applied two-tails Z-tests comparing all pairs of probes.

2.5. Tracers injections and histological procedures

At the end of the recordings, the two probes implanted in each animal were removed and an antero-retrograde neural tracer was injected at the center of the spot previously occupied by each explanted probe. During a surgery under anesthesia (Ketamine, 5 mg/kg i.m. and Medetomidine, 0.08–0.1 mg/kg i.m.), neural tracers were slowly pressure injected at the desired depth through a Hamilton microsyringe (Reno, NV, USA). In the left hemisphere of Mk1 we injected Colera Toxin Subunit B conjugated with Alexa 488 (CTB-g, 1% in phosphate-buffered saline; Molecular Probes) and dextran conjugated with tetramethylrhodamine (Fluoro-Ruby, [FR], 10,000 MW, 10% in 0.1 M phosphate buffer, pH 7.4; Invitrogen-Molecular Probes). In the right hemisphere of Mk2 we injected dextran conjugated with lucifer yellow (Lucifer Yellow Dextrane [LYD], 10,000 MW, 10% in 0.1 M phosphate buffer, pH 7.4; Life Technologies) and FR. After an appropriate survival period for tracer's transport (about 14–21 days), each animal was deeply anesthetized with an overdose of sodium thiopental and perfused through the left cardiac ventricle with saline, 3.5% paraformaldehyde, and 5% glycerol in this order, prepared in phosphate buffer 0.1 M, pH 7.4. Each brain was then blocked coronally on a stereotaxic apparatus, removed from the skull, photographed, and placed in 10% buffered glycerol for 4 days. Finally, each brain was cut frozen into coronal sections of 60 µm thickness and one section of each five was processed to visualize CTB-g, LYD, and FR using the following labeling protocol. After inactivation by the endogenous peroxidase (methanol: hydrogenperoxide = 4:1), selected sections were incubated for 72 h at 4 °C in a primary antibody solution (0.3% Triton and 5% normal goat serum in phosphate buffer solution [PBS]) of rabbit anti-FR or rabbit anti-LY (1:3000; Life Technologies) or rabbit anti-Alexa 488 (1:15000, Life Technologies). Then, they were incubated for 1 h in biotinylated secondary antibody solution (1:200, Vector Laboratories, Burlingame, CA, USA; 0.3% Triton and 5% normal goat serum in PBS). Finally, CTB-g, LYD, and FR labeling was visualized using the Vectastain ABC kit (Vector) and the Vector SG peroxidase substrate kit (SK-4700, Vector) or 3,3′-diaminobenzidine (DAB) as a chromogen. In this latter case the reaction product was intensified with cobalt chloride and nickel ammonium sulfate. For both monkeys, one section of each five was stained using the Nissl method (thionin, 0.1% in 0.1 M acetate buffer, pH 3.7).

The locations of the electrode tracks and of the injection sites were assessed under an optical microscope in Nissl-stained sections and then plotted and digitized together with the outer and inner borders of the cerebral cortex using a computer-based charting system (for the details of the procedure, see Gerbella et al. 2016). The antero-posterior locations of the probes are defined relative to their distance from the anterior commissure (AC), and have been numbered from 1 to 4: the same numbering was adopted to classify the corresponding injection (Fig. 1C). The histologically identified location of the probes is shown on photomicrographs of each injected hemisphere (Figs. S2 and S3).

2.6. Identification and quantification of cortico-cortical and cortico-striatal labeled neurons

The distribution of retrograde cortical labeling was plotted and counted in sections spaced 600 µm apart from each other, together with the outer and inner cortical borders, using the afore mentioned computer based charting system. Data from individual sections were also imported into dedicated software (Bettio et al. 2001) allowing us to create 3D reconstructions of the hemispheres from individual histological sections containing labeled cells. The criteria and maps adopted for attributing the labeling to different brain regions were the same adopted in previous studies (for details see (Lanzilotto et al., 2019; Bruni et al., 2018)). Concerning cortico-cortical projections, we counted all the labeled cells excluding those of area F6 and expressed the cortical afferents to the injected spot of F6 in terms of percentage of labeled neurons found in a given cortical region relative to the total number of labeled cells. Statistical analysis was performed with a chi-square test, comparing the number of neurons observed in each anatomical territory with the value expected if the proportion of observed neurons was uniform across injections at different antero-posterior positions. In addition, to identify the injections-territory combinations mostly contributing to the effect, we computed the adjusted standardized cell residuals (see Table S1).

The projections to the striatum are typically organized in patches of very dense labeled terminals, surrounded by less densely labeled zones: these were designated as "focal" and "diffuse" projections, respectively (Haber et al., 2006). The striatal projections were clearly visible even at relatively low magnification under bright field illumination. Thus, to obtain faithful reproductions of the labeling distribution, the projections were visualized by extracting the labeling from digitalized photographs taken with a ×10 objective (see Calzavara et al., 2007; Borra et al., 2015; Gerbella et al., 2016). Specifically, using Adobe Photoshop (Adobe Systems Incorporated, San Jose, CA, USA) the outlines of the basal ganglia and of adjacent structures were delineated in each photograph on a separate layer. Then, striatal projection fields were selected and converted into a black-and-white image applying a threshold appropriate to extract the labeling, stained in black or blue, from the lighter background. Comparison with the original image ensured that the labeling was accurately extracted and no false positives were included in the image (for further details of this procedure see Fig. 2 of Gerbella et al. 2016). For a quantitative assessment of the focal projections in the striatum we subdivided it in three different territories: the caudate, the anterior putamen (i.e. the sector anterior to the AC, also designated as "associative" putamen) and the posterior putamen

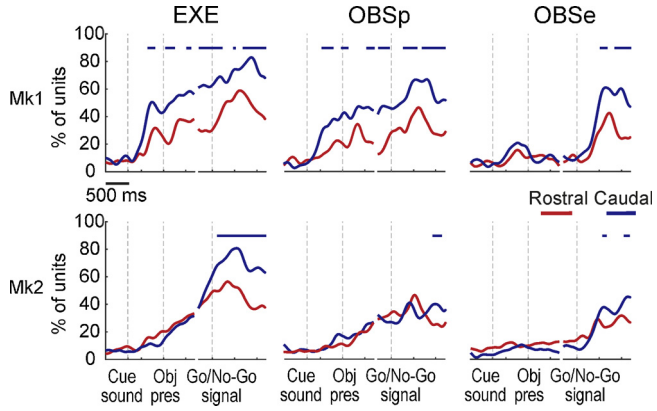

Fig. 2. Tuning properties of units recorded from probes located in different rostro-caudal positions in area F6. Percentage of units with significant tuning for Go/No-Go condition in (from left to right) EXE, OBSp and OBSe. The percentage is expressed relative to the total number of units recorded from the rostral and the caudal probe within each monkey. Colored lines above each plot indicate the time bins where the fraction of tuned units is significantly different between the rostral and the caudal probe (χ^2 $p < 0.05$, uncorrected).

(i.e. the sector posterior to the AC, also designated as "skeletomotor" putamen). Then, we quantified the density of the focal projections in each of these three striatal subdivisions as follows. We quantified the surface of the striatum labeled by focal projections in sections spaced 900 µm, using the measure function of the Nis-element software (Nikon Instruments Inc.). Then, we expressed the density of the focal projections in the anterior putamen, the motor putamen, and the caudate as a percentage of the surface labeled in each of these subdivisions relative to the total striatal surface labeled.

3. Results

Neuronal activity was recorded from four cortical sites at distinct rostro-caudal positions along area F6 of the two monkeys (Fig. 1C), spanning the entire extent of the cytoarchitectonically verified area F6 (Figs. S2 and S3). We extracted both multi- and single unit activity, here defined as "units" (see Materials and Methods) and used all of them in order to better approximate the unbiased sampling of the tracing study subsequently performed on the physiologically characterized sites. We isolated 291 units, of which 100 (34.4%) were classified as single units.

3.1. Non-uniform distribution of neuronal properties along the rostro-caudal extent of *F6*

We isolated 112 units from probe 1 (of which 39 single units), 49 from probe 2 (19 single units), 82 from probe 3 (24 single units) and 48 from probe 4 (18 single units), with a similar percentage of single units isolated from each probe (ranging from 29.3% in probe 3 to 38.8% in probe 2). Then, we compared rostral and caudal subpopulations in each monkey focusing on the factors most prominently represented in the whole data set (Fig. S4A), namely: Go/No-Go condition, task context (EXE, OBSp, OBSe) and task epoch (baseline, cue sound, object presentation, Go/No-Go signal).

Time-resolved repeated measures ANOVA (Fig. 2) revealed that, in both monkeys, the caudal probes show the strongest Go/No-Go tuning in EXE and, in case of Mk2, even in OBSp and OBSe. It is worth to note that units recorded from all probes in both monkeys display different Go/No-Go tuning during the cue period (from cue sound onset to the Go/No-Go signal), with greater tuning in OBSp than in OBSe, particularly in Mk1. Furthermore, the percentage of tuned units progressively increases from baseline to action execution epoch in EXE and OBSp throughout the entire task-unfolding period, especially at the most caudal probe of Mk1. Similarly, object tuning (Fig. S4B) is slightly stronger and more sustained from visual presentation of the target to Go-signal at the caudal probe of Mk1, but it is constrained to the monkey's peripersonal space, as it is absent in OBSe. Importantly, the above described differences appear to be specific for the rostro-caudal direction: indeed, when comparing the tuning properties of the same units grouped based on their dorsal/ventral location (regardless of their rostro-caudal position), we did not find any relevant difference (Fig. S4C).

Next, we directly investigated the neural population dynamics underlying the encoding of task- and/or condition-specific features in F6 by considering the firing rates of all units recorded from each probe as an *N*-dimensional neural state space and performing PCA over these firing rates (see Material and Methods). For each task and condition, we projected the corresponding *N*-dimensional (trial-averaged) neural trajectory onto the plane of the first two PCs, which accounted for a percentage of total variance ranging from 34.7% (probe 2) to 47.8% (probe 3). The resulting two-dimensional trajectories for each probe

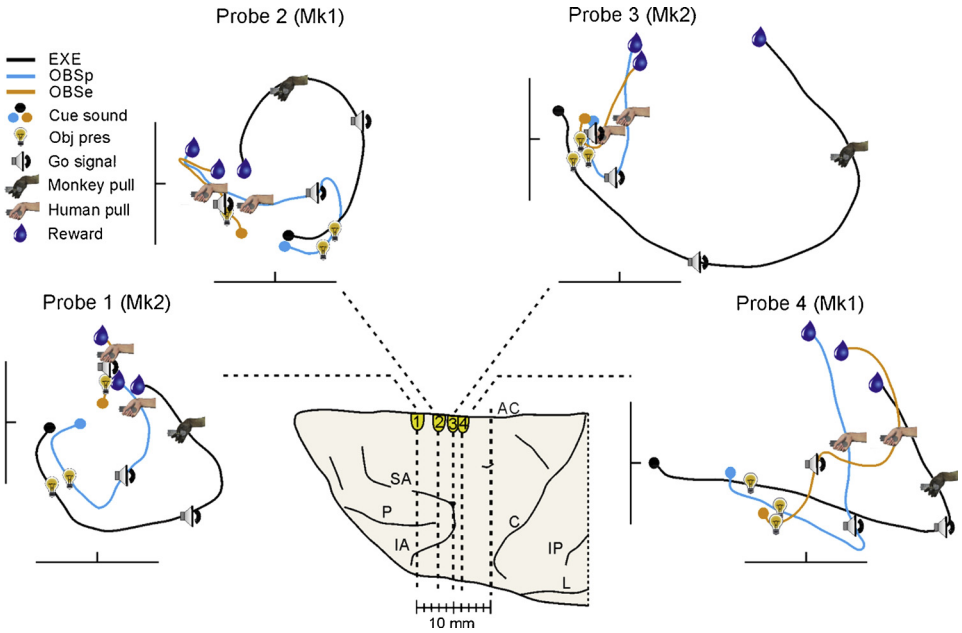

Fig. 3. Local population dynamics along the rostro-caudal extent of area F6. Projection of the neural population response (object averaged) of each probe in the plane defined by the first two principal components during tasks unfolding in the Go conditions of EXE, OBSp and OBSe (see Fig. S5 for analysis of No-Go and grasping-in-the-dark conditions). Each trace represents the projection of the full trial-length activity aligned to Go/No-Go signal. Symbols identify the averaged position of task events along the trial. L, lateral sulcus; IP, intraparietal sulcus; other abbreviations as in Fig. 1.

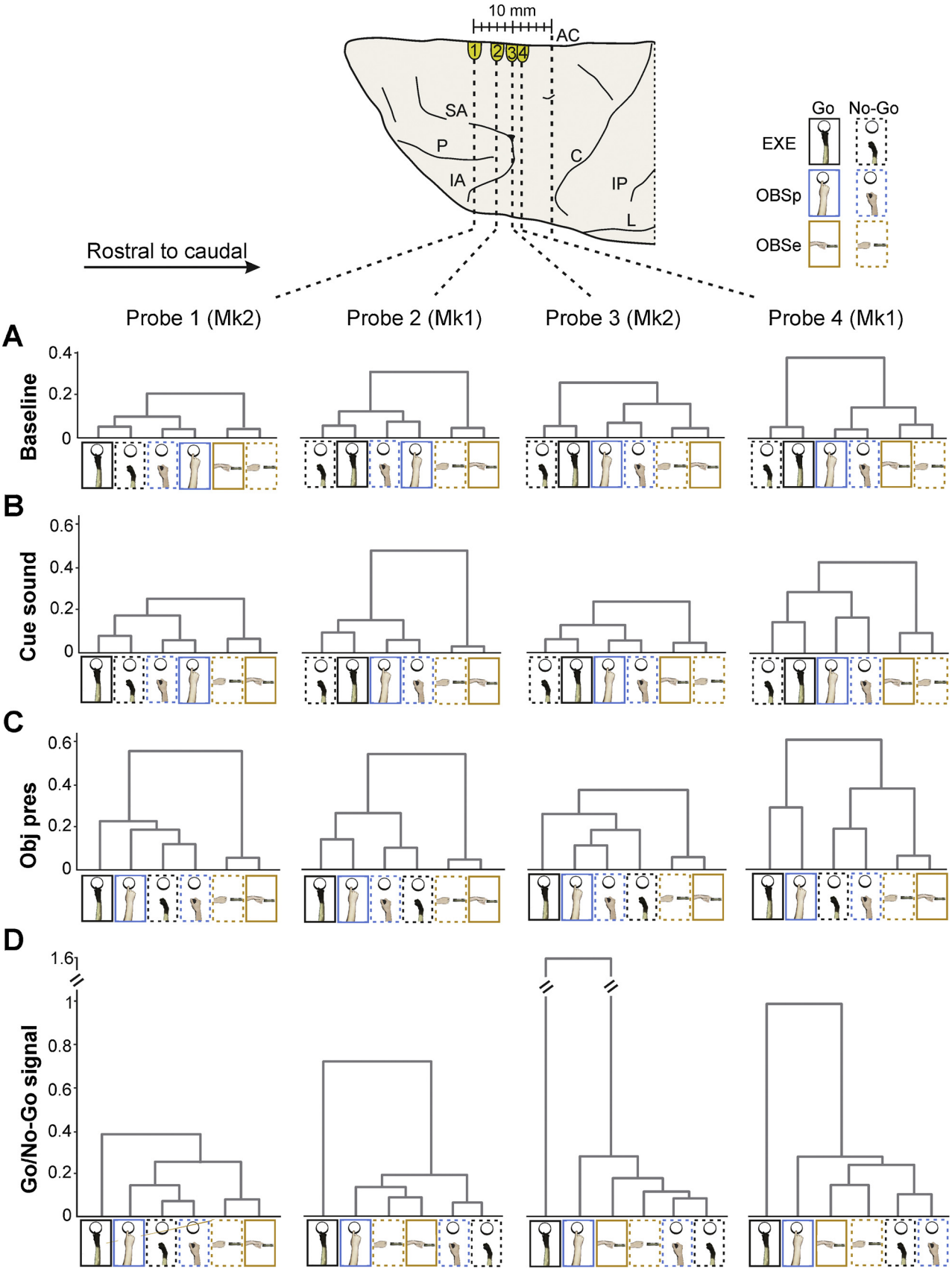

Fig. 4. Neural distances between conditions during specific epochs of the tasks. Dendrograms illustrate the neural distances between conditions during specific epochs (from A to D) of the tasks. Vertical axes indicate Mahalanobis distances between tasks and conditions. Color codes are the same adopted in Fig. 3.

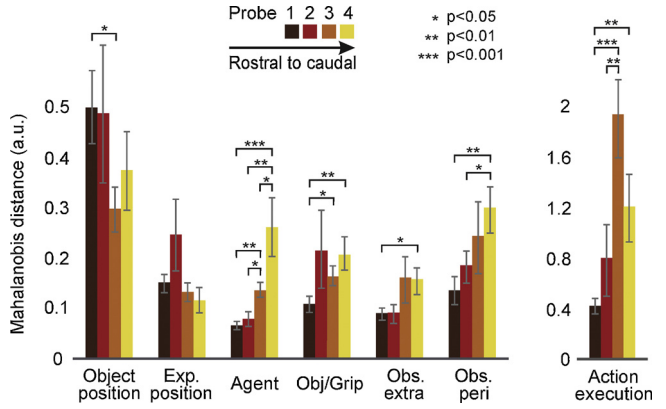

Fig. 5. Functional gradients within F6. Rostro-caudal changes in F6 functional properties, evaluated by computing the neural (Mahalanobis) distance between conditions (see Materials and Methods) based on population activity of each probe (in color code). Histograms represent the population tuning for 1) Object position, 2) Experimenter position, 3) Agent, 4) Object/Grip, 5) Go/No-Go condition in OBSe (Obs extra), 6) Go/No-Go condition in OBSp (Obs Peri), and 7) Go/No-Go condition in EXE (Action execution). Standard errors have been obtained by applying a subsampling procedure and a Z-test has been used to statistically assess significant differences among probes (see Materials and Methods).

(Fig. 3) progress from the start of the trial (colored dots), through object presentation (light bulb), Go/No-Go signal (speaker), object pulling (human and monkey hands) and final reward (blue drop). The starting points and initial trajectories associated with different tasks appear to be clustered differently along the rostro-caudal axis, with greater similarity between EXE and OBSp relative to OBSe, rostrally, and the two OBS tasks relative to EXE, caudally (see Fig. 5 for statistical comparisons). These initial states are followed by two trends emerging during task unfolding in the subpopulations' dynamics along the rostro-caudal axis, which are consistent in both monkeys: 1) an increase in the amplitude of EXE and 2) an increased similarity between the trajectories of the two OBS conditions.

Finally, we performed a hierarchical cluster analysis by computing the Mahalanobis distances (see Materials and Methods) between each pair of conditions of interest (Go/No-Go conditions in all task contexts) in the complete neural state space and presenting the clusters solutions for different epochs as dendrograms (Fig. 4). During baseline epoch (Fig. 4A), the linkage distances among tasks (run in blocks and hence known to the monkey) are greater than those between Go/No-Go conditions within each task (unknown to the monkey before cue sound presentation). In particular, population activity of the two most rostral probes clearly separates task contexts depending on the (near/far) space in which the agent will act. This segregation vanishes moving caudally, where it is replaced by an increasingly clear-cut separation of execution relative to observation tasks (probes 3 and 4), regardless of the space sector in which the observation task is carried out. After cue sound onset (Fig. 4B), all subpopulations consistently segregate the tasks occurring in the monkeys' peripersonal space (EXE and OBSp) from OBSe. Subsequently, during object presentation (Fig. 4C), the overall separation between Go and No-Go conditions increases, and the hierarchical trees undergo local reorganizations, with rostral probes showing a more marked separation between near and far spaces, to which the caudal probe add separation between agents (self/other). Following Go/No-Go signal (Fig. 4D), the various subpopulations exhibit the same general structure of the hierarchical tree, in which monkey's action execution segregates with respects to all the remaining conditions.

The neurophysiological results reveal that area F6 population activity provides information, unevenly distributed along the rostro-caudal extent of the area, about 1) *who is about to act* in a given context (agent-related information), 2) *distance of objects* relative to the monkey (spatial information) and 3) *whether and how the subject will act* (motor information). As a final step, we used Mahalanobis distances in the full-dimensional state space to quantify the local relevance for each of the main functional dimensions (see Materials and Methods) emerged from the previous analyses (Fig. 5). Although all the functional dimensions are represented in all the explored sites, there are clear incremental gradients in the relevance of each dimension along the rostro-caudal (i.e. action execution, agent tuning, observation near and far, object/grip selectivity) and caudo-rostral (i.e. object or experimenter position) direction of area F6.

Next, we addressed whether the local functional specificities here observed can be linked with differential local connectivity patterns.

3.2. Cortical afferences and striatal projections of functionally-characterized spots of *F6*

At end of the neurophysiological experiments, probes were explanted, and antero-retrograde tracers were injected in correspondence of the position of each probe (Fig. 1C). The injections encompass a territory of area F6 ranging, along the antero-posterior axis, from 10 mm rostral to the anterior commissure (AC) in case of injection 1 (corresponding to probe 1) to 4 mm rostral to AC in case of injection 4 (corresponding to probe 4). All the injection sites were completely confined within the cortical grey matter and involved the entire extent of the mesial surface.

All the injections displayed the general connectional fingerprint expected for area F6 (Luppino et al., 1991; Morecraft et al., 2012), consisting in robust connections with frontal lobe regions (i.e. premotor areas from F2 to F7, cingulate cortex and dorsolateral prefrontal areas) and weak connections with parietal areas (including inferior and superior parietal lobule and mesial parietal areas) (see Figs. 6 and S8). The connectivity pattern of F6 injected sectors also showed clear-cut specificities, which reflect the antero-posterior location of the injection site (Fig. 6A). In particular, we observed two main and opposite connectivity gradients, represented by increasingly strong connections with prefrontal (mainly dorsal) areas moving towards the rostral area F6 and increasingly robust connections with premotor and motor cingulate areas moving toward the caudal portion of F6. In the parietal cortex, a relatively stronger labeling was observed after the two more caudal injections in the operculum and in the rostral part of the inferior parietal lobule. Furthermore, denser labeling was observed in medial parietal areas PGm and 31 as well as in posterior parietal area V6A following the most rostral injection (Fig. 6B, S7 and S8). Chi-square tests and adjusted standardized cell residuals analysis showed that the quantitative anatomical differences here observed are statistically significant for almost all the territories here considered (see Table S1).

Since all the tracers injected in this study were antero-retrograde, we could also investigate the distribution of anterograde labeling in the striatum following each injection in area F6 (Fig. 7). The labeling densely involved the territory of the putamen caudal to the AC, deemed to correspond to the hand- and arm-related motor sector (Alexander and de Long 1985; (Nambu, 2011)), as well as the one rostral to the AC, often classified as associative (Alexander et al., 1986; Tremblay et al., 2015). The striatal projections of F6, likewise the cortico-cortical ones, showed a clear rostro-caudal gradient depending on the antero-posterior position of the injected site (Fig. 7A). Specifically, moving from caudal to rostral injection sites in F6, we observed an increase in the labeled terminals within the "associative" putamen as well as in the caudate territories, whereas moving from rostral to caudal injection sites we observed an increase in the cortico-striatal projections ending in the "motor" sector of the putamen (Fig. 7B).

Fig. 8 summarizes the main anatomo-functional associations identified in the present study. The rostral part of F6 exhibits greater specificity than the caudal part in representing the position of objects relative to the monkey, with a clear-cut bias in favor of monkey's

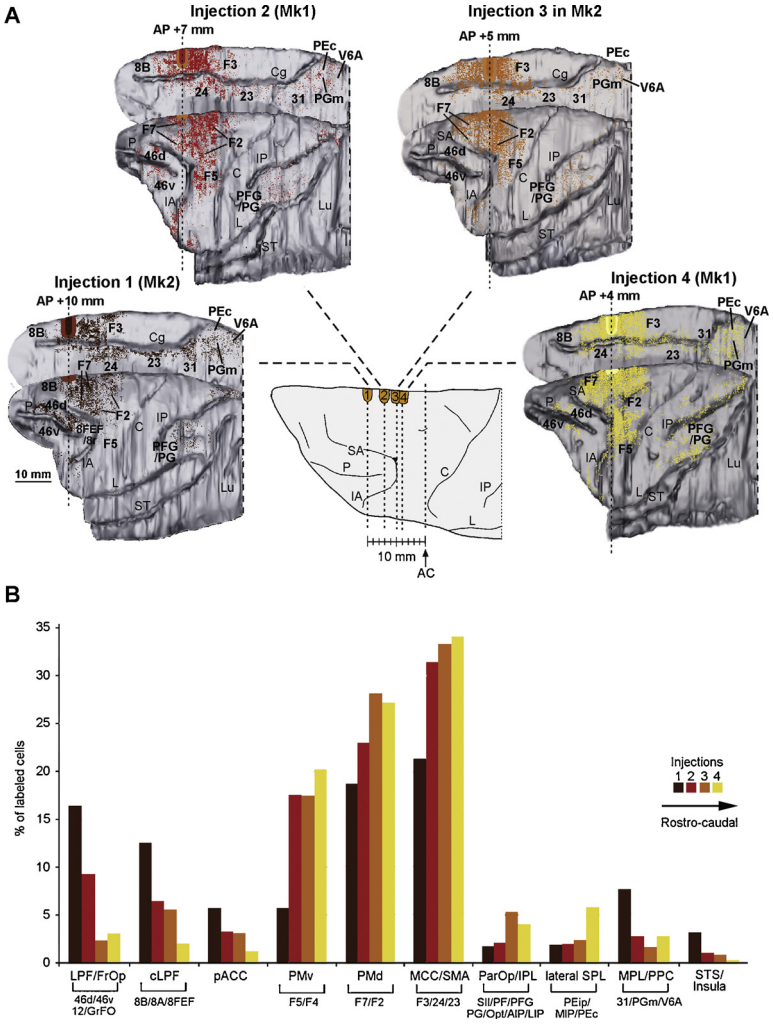

Fig. 6. Anatomical connectivity of F6 sectors located at different antero-posterior positions. (A) Three dimensional anatomical reconstructions illustrating the distribution of labeled cells after injections in four different spots of F6 at different antero-posterior positions. The labeling is shown in dorsolateral and medial views of the injected hemispheres: each dot corresponds to one labeled neuron. The location of each injection is shown as a filled area. Dashed lines indicate the position of the injection site (0 corresponds to the anterior commissure). To facilitate the comparison, all the lateral views of the brain are shown as a left hemisphere and the mesial views as a right hemisphere. The 2D reconstruction in the center is a composite view of all the injection sites, shown as red circles, mapped on a template hemisphere. **(B)** Histograms illustrating the percentage of labeled cells in the various cortical regions following each injection (in color code). The areas (listed under the histogram) are grouped based on anatomo-functional similarity. Abbreviations: ACC, anterior cingulate cortex; Cg, cingulate sulcus; cLPC, caudal lateral prefrontal cortex; FrOp, frontal operculum; IP, intraparietal sulcus; IPL, inferior parietal lobule; LPC, lateral prefrontal cortex; Lu, lunate sulcus; MCC, mesial motor cortex; MPL, medial parietal lobule; ParOp, parietal operculum; PMd, dorsal premotor cortex; PMv, premotor cortex; PPC; posterior parietal cortex; SMA, supplementary motor area; SPL, superior parietal lobule; ST, superior temporal sulcus. Other abbreviations as in Fig. 1.

peripersonal space. These functional specificities are associated with stronger cortical connections with prefrontal, anterior cingulate and mesial parietal regions, as well as with efferences to the caudate nucleus and the anterior putamen in the basal ganglia. In contrast, the caudal part of F6 exhibits remarkable tuning for preparatory and executive aspects of monkey's own reaching-grasping action (i.e. go/no-go tuning, object/grip selectivity) as well as for observed action performed by others in the near and far space. These functional clusters appear to be based on a richer and stronger set of connections with all the lateral and dorsal premotor areas, the superior and inferior parietal lobule, as well as with efferences to the motor putamen in the basal ganglia.

4. Discussion

The agranular frontal cortex lying in the mesial wall of the primates' brain plays a role in a multiplicity of functional domains, such as the processing of spatial (Matzusaka et al. 1992; (Rizzolatti et al., 1990)), contextual (Isoda and Hikosaka, 2007) and social information (Sliwa and Freiwald, 2017; Yoshida et al., 2011; Falcone et al., 2017), and it has been hypothesized that this functional heterogeneity may derive from two possible organizational principles. The classical model (Rizzolatti and Luppino, 2001) supports the existence of discrete anatomo-functional areas (i.e. supplementary and pre-supplementary motor areas), each endowed with its connectional and functional fingerprint, whereas a most recent alternative view (Nachev et al., 2008) maintains that the manifold nature of mesial premotor cortex relies on a rostro-caudal continuum of graded anatomo-functional changes. In the present study, we provide direct anatomo-functional support to this latter view, by showing that the cytoarchitectonically defined pre-supplementary motor area F6 is not homogeneous neither from the functional nor from the connectional point of view. By systematically applying the same set of execution and observation tasks to test neural dynamics in different antero-posterior sites of F6, we found evidence of a variety of functional properties, from spatial information to self and other's action processing. These properties, in spite of the obvious inter-individual variability, appear to form increasing/decreasing gradients along the rostro-caudal axis highly consistent between the two monkeys, paralleled by changes in anatomical connectivity with frontal, parietal and basal ganglia regions. These findings support the view that gradual transitions in connectional and functional properties constitute the basic organizational principle underlying the mapping of functions in the mesial premotor cortex.

Most of the existing neurophysiological studies on mesial frontal regions focused on the identification of an anatomo-functional boundary between the so-called supplementary motor (caudally) and the pre-supplementary motor (rostrally) areas (Luppino et al., 1991; Matsuzaka et al., 1992; Nakamura et al., 1999). However, none of them focused on the possible uneven distribution of the investigated properties within each area. In fact, the findings of some of these studies support the presence of a smooth rostro-caudal change in electrical excitability (Luppino et al., 1991; Matsuzaka et al., 1992), somatosensory and visual responses (Matsuzaka et al., 1992) and agent-specific signals related to motor planning and action execution (Yoshida et al.,

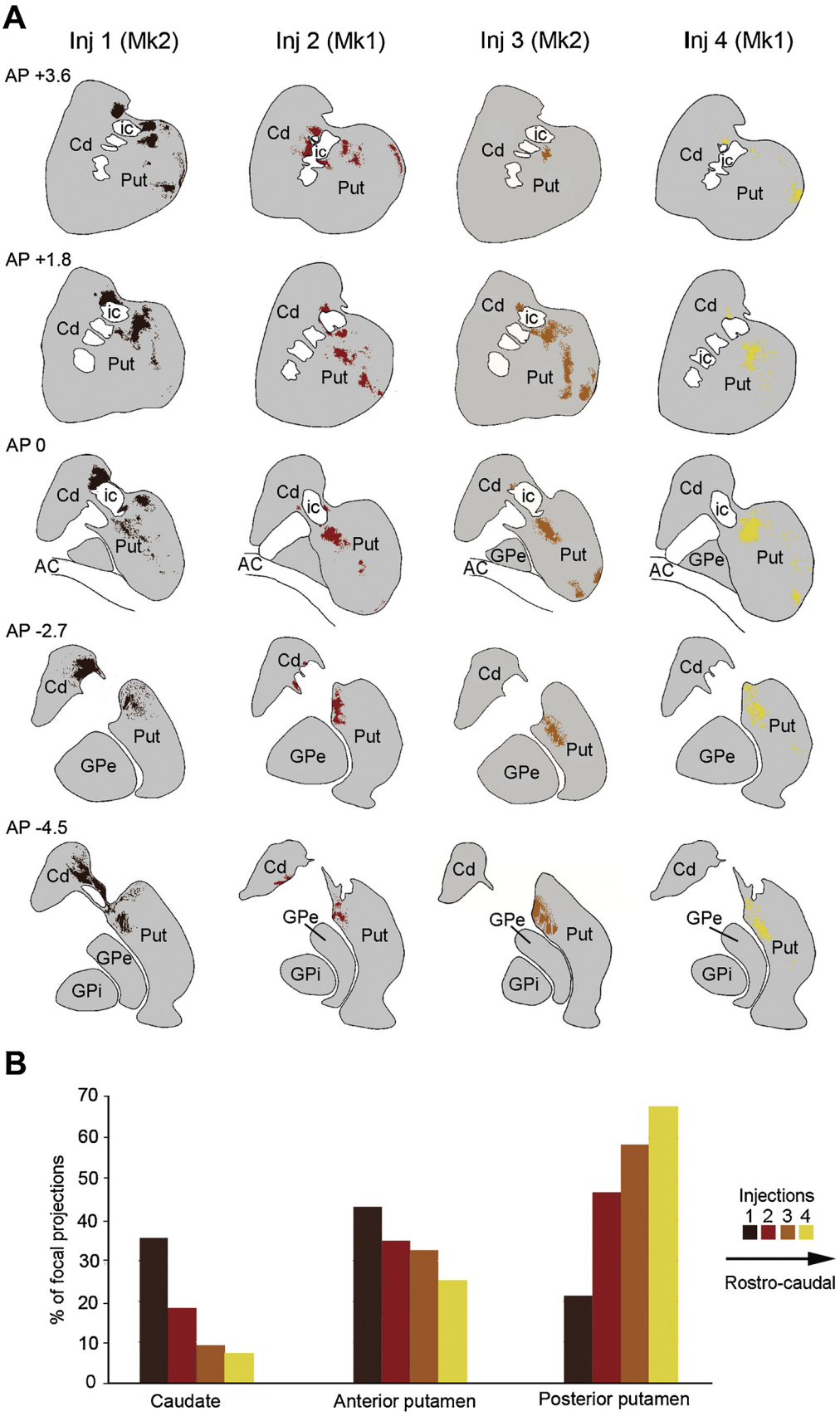

Fig. 7. Striatal projections of F6 sectors located at different antero-posterior positions. (A) Drawings of coronal sections taken at different rostro-caudal positions along the striatum (in row) showing the distribution of the anterograde labeling following injections into different F6 sectors (in column). **(B)** Histograms illustrating the percentage of striatal projections in the three anatomo-functional territories of the striatum defined in the text. Abbreviations: Cd, caudate; GPe, external globus pallidus; GPi, internal globus pallidus; ic, internal capsule; Put, putamen. Other conventions as in Fig. 6.

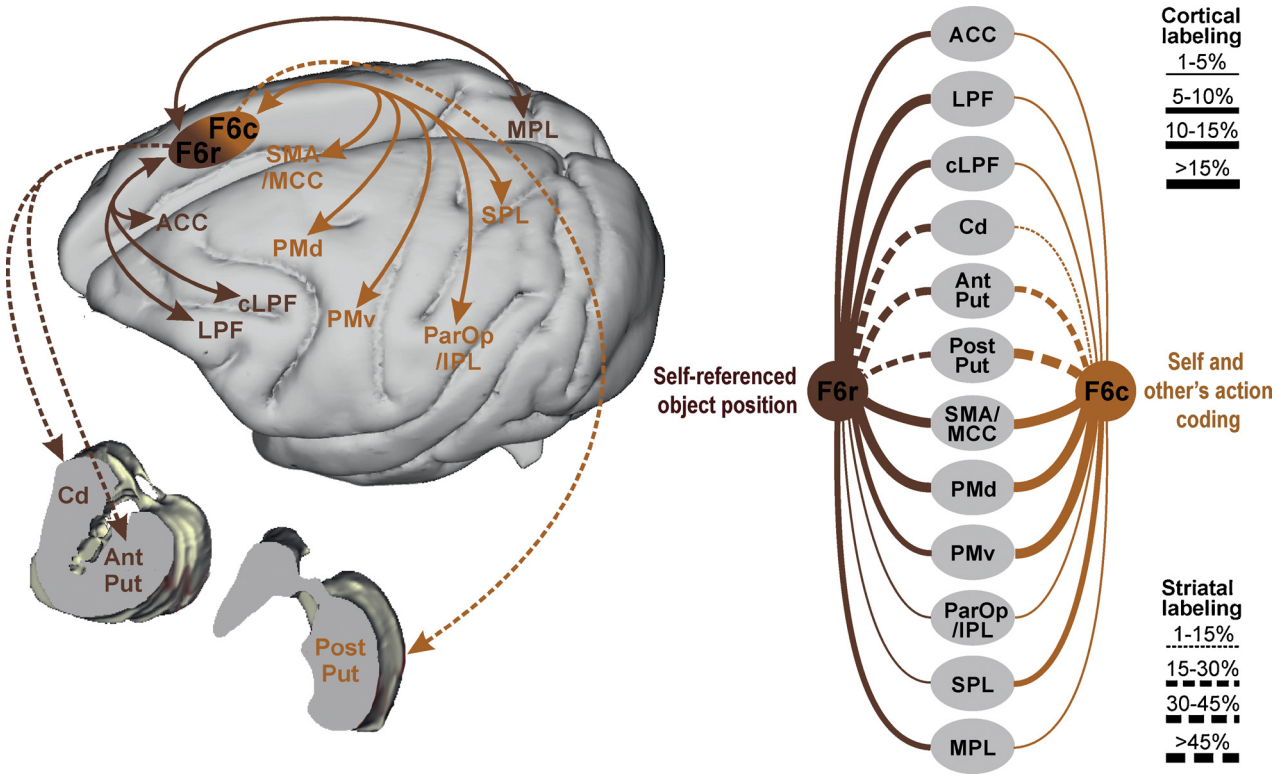

Fig. 8. Schematic representation of the connectivity patterns of rostral and caudal part of area F6. The lines represent the stronger connections observed after the most rostral (injection 1, brown) and caudal (injection 4, orange) injection. The full lines represent the cortical connections, the dashed lines the striatal ones. Conventions and abbreviations as in Figs. 6 and 7.

2011; Falcone et al., 2017). In line with these data, our results show, in the most caudal probes, a stronger tuning for 1) actions executed by the monkey, 2) the type of object that will be grasped, 3) the agent who was expected to act before trial onset, and 4) overtly observed actions independently from the space sector (peri- or extrapersonal) in which these latter occurred. Previous studies also provide some evidence of spatial tuning for left/right location of visual cues and/or direction of arm movements (Matsuzaka et al., 1992), as well as the description of F6 neurons increasing their firing rate when graspable objects approached the monkey (Rizzolatti et al., 1990). Nonetheless, possible uneven rostro-caudal distribution of these spatially tuned neurons was unknown. Here, we found robust evidence of a clear-cut preference for objects located in the monkey's operative space in all the investigated sites of F6. Furthermore, we showed that a preference for the peripersonal space is prevalent in the most rostral probes. Altogether, the evidence of the present study supports the existence of functional gradients in area F6, with its rostral part more tuned to the encoding of distance of objects from the monkey relative to the caudal one, which in turn exhibits stronger tuning to self and other's (observed) action.

The distribution of neuronal properties along the rostro-caudal axis of F6 is paralleled by an even more clear-cut (and consistent between animals) gradient of cortical and striatal connectivity. Indeed, the prevalence of self and others' (observed) action representation and agent tuning prior to trial onset in the caudal part of F6 is paralleled by an increase, in the rostro-caudal direction, of the anatomical connectivity with hand/arm related visuomotor regions of the premotor (F2, F3, F4 and F5), cingulate and lateral parietal/opercular cortices, which host peripersonal ((Graziano et al., 1994; Fogassi et al., 1996); see (Graziano and Cooke, 2006)), mirror ((Gallese et al., 1996; Rozzi et al., 2008; Hihara et al., 2015); see (Bonini, 2017)) and object/grip selective ((Murata et al., 1997; Raos et al., 2006; Bonini et al., 2012; Schaffelhofer and Scherberger, 2016); see (Maranesi et al., 2014)) neurons. This set of connections may extend the well-established role of dorsolateral parieto-frontal regions in the motor representation of self and other's actions ((Gerbella et al., 2017); Bonini 2016) and of the surrounding space (Clery et al., 2015). In addition to the cortical targets, the caudal part of F6 is also linked with the sector of the so-called "motor" putamen, deemed to correspond to forelimb representation (Liles, 1983; Alexander and DeLong, 1985), where set-related activity has been demonstrated (Alexander and Crutcher, 1990). Along the opposite, caudo-rostral direction, increasing tuning for objects located in the monkey's operative space is associated with stronger connections with the dorsolateral prefrontal cortex, deemed to play a pivotal role in coding the spatial location of sensory stimuli (Romanski, 2004; Lanzilotto et al., 2013), the anterior cingulate cortex, playing a role in social decision making processes (Haroush and Williams, 2015), and the mesial posterior parietal cortex, hosting neurons involved in the coupling of visual and motor processing of targets located in the peripersonal space (Hadjidimitrakis et al., 2011; Hadjidimitrakis et al., 2012) and in the processing of potential target objects and other agent's actions (Breveglieri et al., 2019). The stronger link between rostral area F6 and the anterior striatum (caudate nucleus and the anterior putamen) may embed space-constrained representations of objects and agents into cortico-basal ganglia loops devoted to the processing of social context (Klein and Platt, 2013).

Note that space-constrained representations of objects relative to one's own and another's body are widespread along the entire F6. However, they most likely derive from different sources and, hence, different reference frames: the caudal F6, linked with motor-related areas of the lateral parieto-frontal network, may encode a body-centered representation of the peripersonal space, whereas the rostral F6, by virtue of its link with dorsolateral prefrontal and medial parietal cortex, may subserve a more abstract processing of spatial context. Likewise, bimodal (somatosensory and visual) space tuning has been observed in a large territory of the putamen (Graziano and Gross (1993)), which we have shown to be heavily (and unevenly) targeted by

a large territory of area F6, spanning its rostral and caudal sectors. Hence, future studies may unravel differential rostro-caudal trends and tuning properties of striatal neurons devoted to context- or target-specific representations of the peripersonal space. In sum, we evidenced a rostro-caudal organization of cortico-cortical and cortico-basal ganglia connectivity of the monkey pre-supplementary motor area that supports a rostro-caudal distribution of functional properties.

Although, to our knowledge, there is no study explicitly investigating local connectional and functional coupling in mesial frontal regions rostral or caudal to F6, separate lines of evidence in the monkey suggest that at least the connectional trends evidenced in the present study are maintained in mesial frontal territories adjacent to F6. Indeed, mesial frontal areas rostral to F6 (i.e. 8B and 9) exhibit increasingly strong connections with dorsolateral prefrontal, anterior striatal and mesial parietal regions (Calzavara et al., 2007; Eradath et al., 2015; Lanzilotto et al., 2017), whereas the mesial cortex caudal to F6 (i.e. area F3) exhibits increasingly strong connections with somatomotor regions and the caudal putamen, as well as the emergence of direct projections to the spinal cord, which are virtually absent in F6 (Luppino et al., 1993; He et al., 1995; Inase et al., 1999). From the functional point of view, nobody has ever mapped the mesial frontal cortex along the antero-posterior axis using the same task or set of tasks. Nonetheless, existing evidence suggest that area F3 exhibits more markedly motor and somatomotor responses (Picard and Strick, 2003) whereas mesial frontal cortex rostral to F6 operates multisensory integration at a more abstract level and contributes to complex cognitive and decision-making processes (Matsuzaka et al., 2016).

5. Conclusions

Neuroanatomical and neurophysiological data in non-human primates are often used to complement each other, but they are rarely collected in a truly integrated manner that enables the achievement of solid conclusions about anatomo-functional relationship. Consequently, non-human primate literature emphasizes the “discretization” of potentially continuous brain functions. Likewise, functional brain imaging studies in humans tend to produce inherently discretized pictures of brain activity, especially due to technical constraints. However, several recent models support the existence of a rostro-caudal organizational principle of the primates’ brain, with abstract cognitive processes mapped rostrally and sensori-motor behavioral control implemented by the most caudal regions (Petrides, 2005; Koechlin and Summerfield, 2007; Badre and D’Esposito, 2009; Battaglia-Mayer et al., 2016). These models often infer the existence of smooth anatomo-functional changes based on previous data, and this applies to the mesial frontal cortex as well (Nachev et al., 2008). Our study provides direct support to this view, shedding new light on the intrinsic anatomo-functional organization of the pre-supplementary motor area F6 by demonstrating that anatomical and functional transitions smoothly occur in parallel gradients, from visuomotor processing of self and other’s action, caudally, to spatially-committed representation of objects, rostrally. The well-established architectural homology between human and non-human primates’ mesial frontal cortex (Matelli et al., 1991; Nachev et al., 2008; Vorobiev et al., 1998; Ruan et al., 2018) and the evidence of morphological and neurochemical smooth transitions in both species (Geyer et al., 1998; Belmalih et al., 2007), suggest that the anatomo-functional gradients observed here likely represent the anatomo-functional organization principle of the human mesial premotor cortex as well.

Funding

This work was supported by the European Research Council (ERC) under the European Union's Horizon 2020 research and innovation program (ERC starting grant number 678307to L.B), and by the FARE program of the Italian Ministry of Education, Universities and Research (MIUR) (grant number R16PWSFBPL to L.B.).

Declaration of Competing Interest

The authors declare no conflict of interest for this manuscript.

Acknowledgements

We thank Alessia Sepe for drawing the graphical abstract. M.L. is currently supported by an ERC Consolidator grant 2017 (grant agreement 772953).

Appendix A. The Peer Review Overview and Supplementary data

The Peer Review Overview and Supplementary data associated with this article can be found in the online version, at doi:https://doi.org/10.1016/j.pneurobio.2019.101699.

References

Alexander, G.E., Crutcher, M.D., 1990. Preparation for movement: neural representations of intended direction in three motor areas of the monkey. J. Neurophysiol. 64 (1), 133–150. https://doi.org/10.1152/jn.1990.64.1.133.

Alexander, G.E., DeLong, M.R., 1985. Microstimulation of the primate neostriatum. II. Somatotopic organization of striatal microexcitable zones and their relation to neuronal response properties. J. Neurophysiol. 53 (6), 1417–1430. https://doi.org/10.1152/jn.1985.53.6.1417.

Alexander, G.E., DeLong, M.R., Strick, P.L., 1986. Parallel organization of functionally segregated circuits linking basal ganglia and cortex. Annu. Rev. Neurosci. 9, 357–381. https://doi.org/10.1146/annurev.ne.09.030186.002041.

Anderssen, R.S., Brent, R.P., Daley, D.J., Moran, A.P., 1976. Concerning ∫1 0 ··· ∫1 0 (x2 1 ··· x2 k)1/2 dx1 ··· dxk and a Taylor Series Method. SIAM J. Appl. Math. 30 (1), 22–30. https://doi.org/10.1137/0130003.

Badre, D., D’Esposito, M., 2009. Is the rostro-caudal axis of the frontal lobe hierarchical? Nat. Rev. Neurosci. 10 (9), 659–669. https://doi.org/10.1038/nrn2667.

Barz, F., Livi, A., Lanzilotto, M., Maranesi, M., Bonini, L., Paul, O., Ruther, P., 2017. Versatile, modular 3D microelectrode arrays for neuronal ensemble recordings: from design to fabrication, assembly, and functional validation in non-human primates. J. Neural Eng. 14 (3), 036010. https://doi.org/10.1088/1741-2552/aa5a90.

Battaglia-Mayer, A., Babicola, L., Satta, E., 2016. Parieto-frontal gradients and domains underlying eye and hand operations in the action space. Neuroscience 334, 76–92. https://doi.org/10.1016/j.neuroscience.2016.07.009.

Behrens, T.E., Fox, P., Laird, A., Smith, S.M., 2013. What is the most interesting part of the brain? Trends Cogn. Sci. 17 (1), 2–4. https://doi.org/10.1016/j.tics.2012.10.010.

Belmalih, A., Borra, E., Contini, M., Gerbella, M., Rozzi, S., Luppino, G., 2007. A multiarchitectonic approach for the definition of functionally distinct areas and domains in the monkey frontal lobe. J. Anat. 211 (2), 199–211. https://doi.org/10.1111/j.1469-7580.2007.00775.x.

Bonini, L., 2017. The extended mirror neuron network: anatomy, origin, and functions. Neuroscientist 23 (1), 56–67. https://doi.org/10.1177/1073858415626400.

Bonini, L., Maranesi, M., Livi, A., Fogassi, L., Rizzolatti, G., 2014. Space-dependent representation of objects and other’s action in monkey ventral premotor grasping neurons. J. Neurosci. 34 (11), 4108–4119. https://doi.org/10.1523/JNEUROSCI.4187-13.2014.

Bonini, L., Ugolotti Serventi, F., Bruni, S., Maranesi, M., Bimbi, M., Simone, L., Rozzi, S., Ferrari, P.F., Fogassi, L., 2012. Selectivity for grip type and action goal in macaque inferior parietal and ventral premotor grasping neurons. J. Neurophysiol. 108 (6), 1607–1619. https://doi.org/10.1152/jn.01158.2011.

Borra, E., Gerbella, M., Rozzi, S., Luppino, G., 2015. Projections from caudal ventrolateral prefrontal areas to brainstem preoculomotor structures and to Basal Ganglia and cerebellar oculomotor loops in the macaque. Cereb. Cortex 25 (3), 748–764. https://doi.org/10.1093/cercor/bht265.

Breveglieri, R., Vaccari, F.E., Bosco, A., Gamberini, M., Fattori, P., Galletti, C., 2019. Neurons modulated by action execution and observation in the macaque medial parietal cortex. Curr. Biol. 29 (7), 1218–1225. https://doi.org/10.1016/j.cub.2019.02.027. e1213.

Bruni, S., Giorgetti, V., Bonini, L., Fogassi, L., 2015. Processing and integration of contextual information in monkey ventrolateral prefrontal neurons during selection and execution of goal-directed manipulative actions. J. Neurosci. 35 (34), 11877–11890. https://doi.org/10.1523/JNEUROSCI.1938-15.2015.

Bruni, S., Gerbella, M., Bonini, L., Borra, E., Coude, G., Ferrari, P.F., Fogassi, L., Maranesi, M., Roda, F., Simone, L., Serventi, F.U., Rozzi, S., 2018. Cortical and subcortical connections of parietal and premotor nodes of the monkey hand mirror neuron network. Brain Struct. Funct. 223 (4), 1713–1729. https://doi.org/10.1007/s00429-017-1582-0.

Calzavara, R., Mailly, P., Haber, S.N., 2007. Relationship between the corticostriatal terminals from areas 9 and 46, and those from area 8A, dorsal and rostral premotor cortex and area 24c: an anatomical substrate for cognition to action. Eur. J. Neurosci. 26 (7), 2005–2024. https://doi.org/10.1111/j.1460-9568.2007.05825.x.

Clery, J., Guipponi, O., Wardak, C., Ben Hamed, S., 2015. Neuronal bases of peripersonal and extrapersonal spaces, their plasticity and their dynamics: knowns and unknowns. Neuropsychologia 70, 313–326. https://doi.org/10.1016/j.neuropsychologia.2014.

10.022.
Eradath, M.K., Abe, H., Matsumoto, M., Matsumoto, K., Tanaka, K., Ichinohe, N., 2015. Anatomical inputs to sulcal portions of areas 9m and 8Bm in the macaque monkey. Front. Neuroanat. 9, 30. https://doi.org/10.3389/fnana.2015.00030.
Falcone, R., Cirillo, R., Ferraina, S., Genovesio, A., 2017. Neural activity in macaque medial frontal cortex represents others' choices. Sci. Rep. 7 (1), 12663. https://doi.org/10.1038/s41598-017-12822-5.
Ferroni, C.G., Maranesi, M., Livi, A., Lanzilotto, M., Bonini, L., 2017. Comparative performance of linear multielectrode probes and single-tip electrodes for intracortical microstimulation and single-neuron recording in macaque monkey. Front. Syst. Neurosci. 11, 84. https://doi.org/10.3389/fnsys.2017.00084.
Fogassi, L., Gallese, V., Fadiga, L., Luppino, G., Matelli, M., Rizzolatti, G., 1996. Coding of peripersonal space in inferior premotor cortex (area F4). J. Neurophysiol. 76 (1), 141–157. https://doi.org/10.1152/jn.1996.76.1.141.
Fujii, N., Mushiake, H., Tanji, J., 2002. Distribution of eye- and arm-movement-related neuronal activity in the SEF and in the SMA and Pre-SMA of monkeys. J. Neurophysiol. 87 (4), 2158–2166. https://doi.org/10.1152/jn.00867.2001.
Gallese, V., Fadiga, L., Fogassi, L., Rizzolatti, G., 1996. Action recognition in the premotor cortex. Brain 119 (Pt 2), 593–609.
Gerbella, M., Rozzi, S., Rizzolatti, G., 2017. The extended object-grasping network. Exp. Brain Res. 235 (10), 2903–2916. https://doi.org/10.1007/s00221-017-5007-3.
Gerbella, M., Borra, E., Mangiaracina, C., Rozzi, S., Luppino, G., 2016a. Corticostriate projections from areas of the "Lateral grasping network": evidence for multiple hand-related input channels. Cereb. Cortex 26 (7), 3096–3115. https://doi.org/10.1093/cercor/bhv135.
Gerbella, M., Borra, E., Rozzi, S., Luppino, G., 2016b. Connections of the macaque Granular Frontal Opercular (GrFO) area: a possible neural substrate for the contribution of limbic inputs for controlling hand and face/mouth actions. Brain Struct. Funct. 221 (1), 59–78. https://doi.org/10.1007/s00429-014-0892-8.
Geyer, S., Matelli, M., Luppino, G., Schleicher, A., Jansen, Y., Palomero-Gallagher, N., Zilles, K., 1998. Receptor autoradiographic mapping of the mesial motor and premotor cortex of the macaque monkey. J. Comp. Neurol. 397 (2), 231–250.
Graziano, M.S., Cooke, D.F., 2006. Parieto-frontal interactions, personal space, and defensive behavior. Neuropsychologia 44 (13), 2621–2635.
Graziano, M.S., Gross, C.G., 1993. A bimodal map of space: somatosensory receptive fields in the macaque putamen with corresponding visual receptive fields. Exp. Brain Res. 97 (1), 96–109.
Graziano, M.S., Yap, G.S., Gross, C.G., 1994. Coding of visual space by premotor neurons. Science 266 (5187), 1054–1057.
Haber, S.N., Kim, K.S., Mailly, P., Calzavara, R., 2006. Reward-related cortical inputs define a large striatal region in primates that interface with associative cortical connections, providing a substrate for incentive-based learning. J. Neurosci. 26 (32), 8368–8376. https://doi.org/10.1523/JNEUROSCI.0271-06.2006.
Hadjidimitrakis, K., Breveglieri, R., Placenti, G., Bosco, A., Sabatini, S.P., Fattori, P., 2011. Fix your eyes in the space you could reach: neurons in the macaque medial parietal cortex prefer gaze positions in peripersonal space. PLoS One 6 (8), e23335. https://doi.org/10.1371/journal.pone.0023335.
Hadjidimitrakis, K., Breveglieri, R., Bosco, A., Fattori, P., 2012. Three-dimensional eye position signals shape both peripersonal space and arm movement activity in the medial posterior parietal cortex. Front. Integr. Neurosci. 6, 37. https://doi.org/10.3389/fnint.2012.00037.
Haroush, K., Williams, Z.M., 2015. Neuronal prediction of opponent's behavior during cooperative social interchange in primates. Cell 160 (6), 1233–1245. https://doi.org/10.1016/j.cell.2015.01.045.
He, S.Q., Dum, R.P., Strick, P.L., 1995. Topographic organization of corticospinal projections from the frontal lobe: motor areas on the medial surface of the hemisphere. J. Neurosci. 15 (5 Pt 1), 3284–3306.
Hihara, S., Taoka, M., Tanaka, M., Iriki, A., 2015. Visual responsiveness of neurons in the secondary somatosensory area and its surrounding parietal operculum regions in awake macaque monkeys. Cereb. Cortex 25 (11), 4535–4550. https://doi.org/10.1093/cercor/bhv095.
Inase, M., Tokuno, H., Nambu, A., Akazawa, T., Takada, M., 1999. Corticostriatal and corticosubthalamic input zones from the presupplementary motor area in the macaque monkey: comparison with the input zones from the supplementary motor area. Brain Res. 833 (2), 191–201.
Isoda, M., Hikosaka, O., 2007. Switching from automatic to controlled action by monkey medial frontal cortex. Nat. Neurosci. 10 (2), 240–248. https://doi.org/10.1038/nn1830.
Johansen-Berg, H., Behrens, T.E., Robson, M.D., Drobnjak, I., Rushworth, M.F., Brady, J.M., Smith, S.M., Higham, D.J., Matthews, P.M., 2004. Changes in connectivity profiles define functionally distinct regions in human medial frontal cortex. Proc. Natl. Acad. Sci. U. S. A. 101 (36), 13335–13340. https://doi.org/10.1073/pnas.0403743101.
Klein, J.T., Platt, M.L., 2013. Social information signaling by neurons in primate striatum. Curr. Biol. 23 (8), 691–696. https://doi.org/10.1016/j.cub.2013.03.022.
Koechlin, E., Summerfield, C., 2007. An information theoretical approach to prefrontal executive function. Trends Cogn. Sci. 11 (6), 229–235. https://doi.org/10.1016/j.tics.2007.04.005.
Lanzilotto, M., Livi, A., Maranesi, M., Gerbella, M., Barz, F., Ruther, P., Fogassi, L., Rizzolatti, G., Bonini, L., 2016. Extending the cortical grasping network: pre-supplementary motor neuron activity during vision and grasping of objects. Cereb. Cortex 26 (12), 4435–4449. https://doi.org/10.1093/cercor/bhw315.
Lanzilotto, M., Ferroni, C.G., Livi, A., Gerbella, M., Maranesi, M., Borra, E., Passarelli, L., Gamberini, M., Fogassi, L., Bonini, L., Orban, G.A., 2019. Anterior intraparietal area: a hub in the observed manipulative action network. Cereb. Cortex 29 (4), 1816–1833. https://doi.org/10.1093/cercor/bhz011.
Lanzilotto, M., Perciavalle, V., Lucchetti, C., 2013. A new field in monkey's frontal cortex: premotor ear-eye field (PEEF). Neurosci. Biobehav. Rev. 37 (8), 1434–1444. https://doi.org/10.1016/j.neurobiorev.2013.05.010.
Lanzilotto, M., Gerbella, M., Perciavalle, V., Lucchetti, C., 2017. Neuronal encoding of self and others' head rotation in the macaque dorsal prefrontal cortex. Sci. Rep. 7 (1), 8571. https://doi.org/10.1038/s41598-017-08936-5.
Liles, S.L., 1983. Activity of neurons in the putamen associated with wrist movements in the monkey. Brain Res. 263 (1), 156–161.
Livi, A., Lanzilotto, M., Maranesi, M., Fogassi, L., Rizzolatti, G., Bonini, L., 2019. Agent-based representations of objects and actions in the monkey pre-supplementary motor area. Proc. Natl. Acad. Sci. U. S. A. 116 (7), 2691–2700. https://doi.org/10.1073/pnas.1810890116.
Luppino, G., Matelli, M., Camarda, R.M., Gallese, V., Rizzolatti, G., 1991. Multiple representations of body movements in mesial area 6 and the adjacent cingulate cortex: an intracortical microstimulation study in the macaque monkey. J. Comp. Neurol. 311 (4), 463–482. https://doi.org/10.1002/cne.903110403.
Luppino, G., Matelli, M., Camarda, R., Rizzolatti, G., 1993. Corticocortical connections of area F3 (SMA-proper) and area F6 (pre-SMA) in the macaque monkey. J. Comp. Neurol. 338 (1), 114–140. https://doi.org/10.1002/cne.903380109.
Maranesi, M., Bonini, L., Fogassi, L., 2014. Cortical processing of object affordances for self and others' action. Front. Psychol. 5, 538. https://doi.org/10.3389/fpsyg.2014.00538.
Matelli, M., Luppino, G., Rizzolatti, G., 1991. Architecture of superior and mesial area 6 and the adjacent cingulate cortex in the macaque monkey. J. Comp. Neurol. 311 (4), 445–462. https://doi.org/10.1002/cne.903110402.
Matsuzaka, Y., Aizawa, H., Tanji, J., 1992. A motor area rostral to the supplementary motor area (presupplementary motor area) in the monkey: neuronal activity during a learned motor task. J. Neurophysiol. 68 (3), 653–662. https://doi.org/10.1152/jn.1992.68.3.653.
Matsuzaka, Y., Tanji, J., Mushiake, H., 2016. Representation of behavioral tactics and tactics-action transformation in the primate medial prefrontal cortex. J. Neurosci. 36 (22), 5974–5987. https://doi.org/10.1523/JNEUROSCI.4572-15.2016.
Morecraft, R.J., Stilwell-Morecraft, K.S., Cipolloni, P.B., Ge, J., McNeal, D.W., Pandya, D.N., 2012. Cytoarchitecture and cortical connections of the anterior cingulate and adjacent somatomotor fields in the rhesus monkey. Brain Res. Bull. 87 (4–5), 457–497. https://doi.org/10.1016/j.brainresbull.2011.12.005.
Murata, A., Fadiga, L., Fogassi, L., Gallese, V., Raos, V., Rizzolatti, G., 1997. Object representation in the ventral premotor cortex (area F5) of the monkey. J. Neurophysiol. 78 (4), 2226–2230. https://doi.org/10.1152/jn.1997.78.4.2226.
Nachev, P., Kennard, C., Husain, M., 2008. Functional role of the supplementary and pre-supplementary motor areas. Nat. Rev. Neurosci. 9 (11), 856–869. https://doi.org/10.1038/nrn2478.
Nakamura, K., Sakai, K., Hikosaka, O., 1999. Effects of local inactivation of monkey medial frontal cortex in learning of sequential procedures. J. Neurophysiol. 82 (2), 1063–1068. https://doi.org/10.1152/jn.1999.82.2.1063.
Nambu, A., 2011. Somatotopic organization of the primate Basal Ganglia. Front. Neuroanat. 5, 26. https://doi.org/10.3389/fnana.2011.00026.
Petrides, M., 2005. Lateral prefrontal cortex: architectonic and functional organization. Philos. Trans. R. Soc. Lond. B Biol. Sci. 360 (1456), 781–795. https://doi.org/10.1098/rstb.2005.1631.
Picard, N., Strick, P.L., 1996. Motor areas of the medial wall: a review of their location and functional activation. Cereb. Cortex 6 (3), 342–353.
Picard, N., Strick, P.L., 2001. Imaging the premotor areas. Curr. Opin. Neurobiol. 11 (6), 663–672.
Picard, N., Strick, P.L., 2003. Activation of the supplementary motor area (SMA) during performance of visually guided movements. Cereb. Cortex 13 (9), 977–986.
Raos, V., Umilta, M.A., Murata, A., Fogassi, L., Gallese, V., 2006. Functional properties of grasping-related neurons in the ventral premotor area F5 of the macaque monkey. J. Neurophysiol. 95 (2), 709–729. https://doi.org/10.1152/jn.00463.2005.
Rizzolatti, G., Luppino, G., 2001. The cortical motor system. Neuron 31 (6), 889–901.
Rizzolatti, G., Gentilucci, M., Camarda, R.M., Gallese, V., Luppino, G., Matelli, M., Fogassi, L., 1990. Neurons related to reaching-grasping arm movements in the rostral part of area 6 (area 6a beta). Exp. Brain Res. 82 (2), 337–350.
Romanski, L.M., 2004. Domain specificity in the primate prefrontal cortex. Cogn. Affect. Behav. Neurosci. 4 (4), 421–429.
Rozzi, S., Ferrari, P.F., Bonini, L., Rizzolatti, G., Fogassi, L., 2008. Functional organization of inferior parietal lobule convexity in the macaque monkey: electrophysiological characterization of motor, sensory and mirror responses and their correlation with cytoarchitectonic areas. Eur. J. Neurosci. 28 (8), 1569–1588. https://doi.org/10.1111/j.1460-9568.2008.06395.x.
Ruan, J., Bludau, S., Palomero-Gallagher, N., Caspers, S., Mohlberg, H., Eickhoff, S.B., Seitz, R.J., Amunts, K., 2018. Cytoarchitecture, probability maps, and functions of the human supplementary and pre-supplementary motor areas. Brain Struct. Funct. 223 (9), 4169–4186. https://doi.org/10.1007/s00429-018-1738-6.
Schaffelhofer, S., Scherberger, H., 2016. Object vision to hand action in macaque parietal, premotor, and motor cortices. Elife 5. https://doi.org/10.7554/eLife.15278.
Shima, K., Mushiake, H., Saito, N., Tanji, J., 1996. Role for cells in the presupplementary motor area in updating motor plans. Proc. Natl. Acad. Sci. U. S. A. 93 (16), 8694–8698.
Sliwa, J., Freiwald, W.A., 2017. A dedicated network for social interaction processing in the primate brain. Science 356 (6339), 745–749. https://doi.org/10.1126/science.aam6383.
Tanji, J., 2001. Sequential organization of multiple movements: involvement of cortical motor areas. Annu. Rev. Neurosci. 24, 631–651. https://doi.org/10.1146/annurev.neuro.24.1.631.
Tanji, J., Shima, K., 1994. Role for supplementary motor area cells in planning several

movements ahead. Nature 371 (6496), 413–416. https://doi.org/10.1038/371413a0.
Tremblay, L., Worbe, Y., Thobois, S., Sgambato-Faure, V., Feger, J., 2015. Selective dysfunction of basal ganglia subterritories: from movement to behavioral disorders. Mov. Disord. 30 (9), 1155–1170. https://doi.org/10.1002/mds.26199.
Vorobiev, V., Govoni, P., Rizzolatti, G., Matelli, M., Luppino, G., 1998. Parcellation of human mesial area 6: cytoarchitectonic evidence for three separate areas. Eur. J. Neurosci. 10 (6), 2199–2203.
Yoshida, K., Saito, N., Iriki, A., Isoda, M., 2011. Representation of others' action by neurons in monkey medial frontal cortex. Curr. Biol. 21 (3), 249–253. https://doi.org/10.1016/j.cub.2011.01.004.
Zapparoli, L., Seghezzi, S., Scifo, P., Zerbi, A., Banfi, G., Tettamanti, M., Paulesu, E., 2018. Dissecting the neurofunctional bases of intentional action. Proc. Natl. Acad. Sci. U. S. A. 115 (28), 7440–7445. https://doi.org/10.1073/pnas.1718891115.